8th Int. Symp. "Nanostructures: Physics and Technology"
St Petersburg, Russia, June 19–23, 2000

QWR/QD.23p

On depolarisation in 0D systems: Lamb-like level shift

Slava V. Rotkin
Ioffe Physico-Technical Institute, St Petersburg, Russia
Beckman Institute, UIUC, 405 N.Mathews, Urbana, IL 61801, USA

Abstract. An extremely quantized 0D system is studied for better understanding of an importance of many-body corrections to an one-electron spectrum. A new approach is proposed to describe the correction appearing as a depolarisation level shift of a (confined) electron moving within an electric field of a (confined) collective mode. For a quantum dot the correction diminishes at the size about 10^4-10^5 atoms, depending also on other system parameters. For a closed-shell carbon cluster the effect does not depend on the cluster size owing to stronger quantization and the one-electron estimation does not fit anywhere. For the semiconductor quantum dot system an experimental method to check the depolarisation model is proposed.

In the paper we study an anomalous large level shift, resulted from the interaction of an electron in a 0D-system with zero-point oscillations of confined modes of the electric field. Of course, any complete many-body theory, taking into account all the Coulomb interaction, gives the correct value for the electron levels, though it is not known for present. We go to reveal an important correction treating the effect of valence electrons of a 0D object, which can be a spherical quantum dot and a closed-shell fullerene cluster, selfconsistently. Then the theory remains to be semi-classical while a nature of the effect is quantum-electrodynamical. This continues our consideration of C_{60} in frame of a simple quantum mechanical model of the spherical-shell quantum well (SSQW) [1].

The energy correction depends on the system radius. This size scaling of the depolarisation is computed within an approach proposed by Migdal [2] for a calculation of Lamb shift in a hydrogen-like atom. The shift of the one-electron level is quite predictable and we will show that its amount becomes very large for the quantized system. The closed-shell fullerene depolarisation is of the order of the bare energy and independent of the cluster radius while the shift in the quantum dot decreases with the increasing number of atoms. Between two examples — a fullerene carbon nanocluster and a semiconductor quantum dot structure — the latter has not only theoretical importance. The possible experimental manifestation of the depolarisation effect is proposed basing on the spectroscopy of the quantum dot levels for different matrix materials.

1. Theory for depolarisation level shift: C_{60}

1. The use of the group of full rotations, SO(3), allows one to label the one-electron states and to get analytically the solution for the selfconsistent RPA response function of C_{60} [1]. A peak of a collective excitation shows up in this spectrum, resulting from fast coherent oscillations of a total electron density of valence states. This surface density oscillation can be thought as a confined electrical field mode or the surface plasmon.

We have considered semiclassically the LS for an arbitrary shell object in [3], followed to Migdal [2]. The frequency of the zero-point fluctuations of the external field is much

higher than the inverse period of the electron orbit $\omega_p \gg \pi/\tau$. Therefore, the adiabatic approximation has to be used and one divides the fast (field) and slow (electron) variables. An electron is subjected to short fast deflections from its original orbit in the high-frequency field of the electromagnetic wave of the zero-point fluctuation. Then the energy shift is given by the second order perturbation theory as

$$\delta E = \langle H(r+\delta) - H(r)\rangle = \left\langle \nabla H \cdot \vec{\delta} + \frac{1}{2}\nabla^2 H\ \vec{\delta}\cdot\vec{\delta} + \ldots \right\rangle = \frac{1}{4}\nabla^2 H\ \overline{\delta^2} + o(\overline{\delta^2}) \quad (1)$$

where $H(r)$ is the unperturbed Hamiltonian and $H(r+\delta)$ is the Hamiltonian with account for the random electron deflection δ. The angle brackets represent the quantum mechanical average over the fast variables of the field (or, the same, over the random electron deflections). The perturbed Hamiltonian is expanded in series on the δ and a first nonzero contribution is taken.

The expression for the mean square of the deflection, $\overline{\delta^2}$ was deduced in Ref. [3]. Though the estimation is semiquantitative, the deflection is of the order of atomic unit, $a_B \simeq 0.53$ Å. The $\overline{\delta^2}$ in the SSQW does not depend on the radius, neither on the number of atoms because of the density of the valence electrons is the same.

Let suppose that one-electron model works for some cluster C_N. The one-electron Hamiltonian reads as [1]:

$$H_o = E_n + \hbar^2/2mR^2\ \hat{L}^2, \quad (2)$$

where E_n is the energy of a lowest level of n-th radial series; an orbital quantization energy $\hbar^2/mR^2$ defines the SO(3) level spacing between eigenstates of the angular momentum operator. The SSQW level shift reads as follows:

$$E_L = E_L^{(0)}\left(1 + \kappa\hat{L}^2/N\right), \quad (3)$$

where $\kappa \sim 0.36$ is the numerical coefficient depending only on b, the carbon bond length: $\kappa = \sqrt{a_B/b}\pi^2/2^{2.5}/3$.

2. Within the closed-shell model the optical gap occurs between the levels $|L_F\rangle$ and $|L_F+1\rangle$. Within the closed-shell approximation the Fermi momentum fulfills the condition $N = 2\sum_{L=0}^{L_F}(2L+1) = 2(L_F+1)^2$. The gap value does depend on the cluster size, decreasing to the zero as N going to infinity in order to approach the gapless graphite.

The depolarisation makes the gap wider. The renormalisation is universal for any closed-shell spherical cluster and amounts about 40% to the bare value:

$$E_g = E_g^{(0)}(1+\kappa) \simeq 1.36E_g^{(0)}. \quad (4)$$

where the parameter $\kappa \simeq 0.36$ is the same as before.

2. Depolarisation energy level shift in QD structure

1. In order to evaluate the LS for the quantum dot (QD) the simplified *spherical* model in frame of an *effective mass* approximation was applied. The size scaling of the depolarisation shift is not sensitive to the model used, being dependent mainly on the corresponding density of states of the collective modes.

The simplest QD Hamiltonian is considered to have only the rotational correction which reads as:

$$\delta H = \frac{\hat{L}^2}{2mR^2}\left(-2\frac{\delta}{R} + 3\frac{\delta^2}{R^2} + \ldots\right) \quad (5)$$

where R is about the spherical QD radius; m is the electron mass which is supposed to be constant within the dot; $\hat{L}$ is the angular momentum operator.

Nearly self-evidently the bulk plasmon shift is negligible. The small factor, contained in the 3D LS, comes essentially from the expression for $\overline{\delta^2}$ which scales as $1/N$ [3], where N is the number of atoms in the QD. The mean square deflection, caused by the 3D mode (which is not confined at all), decreases with N too rapidly.

The square of the deflection [3] $\overline{\delta^2} = e^2/4m^2 \int d^3k \ \mathcal{E}_k^2/\omega_k^4$ is proportional to the square of the electric field strength. The field strength can be rewritten as the zero-point oscillation frequency $\mathcal{E}_k^2 = 2\pi\hbar\omega_k$ through the quantized field normalisation. The 3D plasmon frequency does not depend on the quantum number $\mathbf{k}$. Hence, the mean square deflection contains the total number of states effecting on the electron level in the QD. The integral is limited above by $k_{\max} \sim 1/R$. In 3D-case it brings the factor $R^{-3} \sim N^{-1}$ claimed in the beginning of the section. Then the depolarisation level shift due to 3D modes scales with N as follows:

$$\Delta_{3D} = \frac{\delta E}{E^{(0)}} \propto N^{-5/3}. \tag{6}$$

The rude estimation of the prefactor shows that even for the small QD with $N = 100$ the shift is 10^{-6} of the bare energy and will not be resolved because of a number of other different factors effecting the level position.

To give a complete picture, the standard LS due to the zero-point oscillations of the free electromagnetic modes of the vacuum reads as follows: $\Delta_{\text{vac}} \propto \alpha^3 N^{-2/3}$, where $\alpha \simeq 1/137$ is the fine structure constant. Though the slope of the LS in N is much slower than in Eq. (6) the prefactor is tiny because of α^3.

2. Two possible candidates for the confined plasmon modes in the QD system are the 2D plasmon and the 0D spherical mode. The former mode can arise because of some interface possibly grown within the structure (see inset in Fig. 1). It might be a wetting layer, if it is thick enough to confine the electromagnetic field. The 2D plasmon naturally originates at the boundary between the semiconductor structure and a distinct substrate. The scaling in N will have a lower exponent that reflects the different density of the confined field (plasmon) states: $\Delta_{2D} \propto N^{-7/6}$. The shift depends on the inverse size nearly linearly. However, the prefactor dominates at some moderate size of the QD and lessens the LS to 10^{-3} for $N = 100$. The depolarisation is still to be too small to expect experimental consequences.

3. The $\overline{\delta^2}$ considered above the less, the larger the QD size, that is not the case for the deflection due to completely localized modes like in Sec. 1. In this section the localized modes are the surface plasmons of the spherical inclusion (with the dielectric function ϵ_1) in the matrix (with the different dielectric function ϵ_2). $\Delta \propto N^{-2/3}$. Our estimation shows that the level correction, becoming of the order of 50%, plays the important role for the QD of 100 atoms and smaller. We collected all studied contributions to the depolarisation LS and plot them in the log–log scale versus the QD size in Fig. 1.

The depolarisation because of the localized surface QD modes is large enough to propose an experiment supporting our model. It is easy to check that $\overline{\delta^2} \sim \omega_{\text{L}}^{-3}$, which is nearly the frequency of the bulk plasmon in the matrix (with the weak dependence on the mode angular momentum, see [3]). Therefore, changing the optical properties of the matrix surrounding the QD, one shifts the levels. If the bare energy level lies deep in the potential well, its position is nearly independent of the well depth which changes along with the matrix parameters. The deep bare level energy depends only on the well width. Hence, the depolarisation LS is distinguishable from the standard space quantization LS.

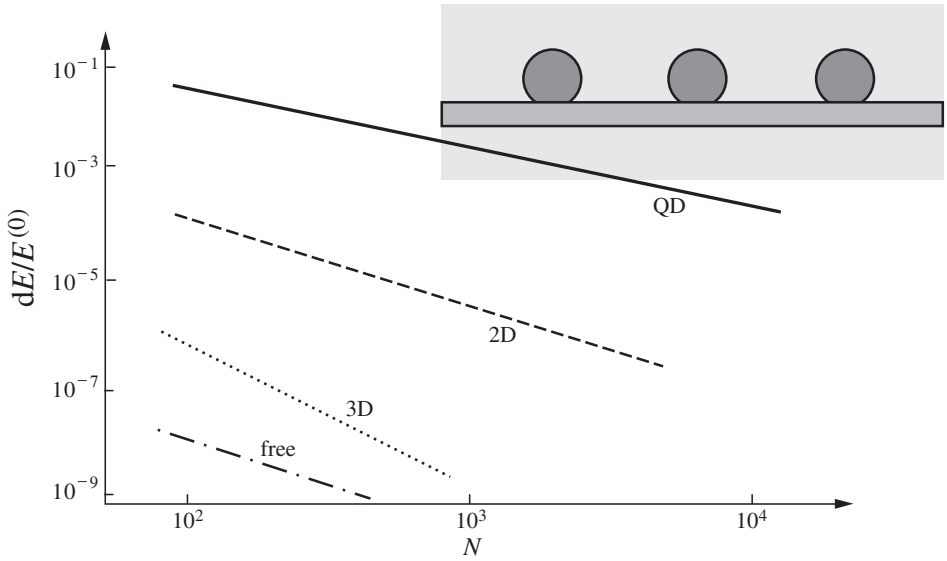

Fig. 1. The level shift of the QD electron, calculated for 4 different depolarisation mechanisms. The slopes and the prefactors of these depolarisation shifts were derived analytically. Inset: The scheme of the QD structure to model.

In summary, the effect of the zero-point oscillations of the free and confined electromagnetic field on the level of the confined electron in the 0D-system, as the closed-shell carbon cluster and the spherical QD, is studied. The depolarisation due to an interaction with the zero-point fluctuations shifts up the bare one-electron state. The gap renormalisation, which follows from the angular momentum dependent LS in the fullerene cluster, is shown to be independent of the fullerene radius. The size dependence of LS in the QDs is different for 4 modes considered in the paper. Although, in general, the depolarisation decreases with the QD size, the **localized** surface electromagnetic mode results in the essential level shift and is to be possibly resolved experimentally for a QD made from some hundreds atoms. Another method to detect the effect could be a measurement of a deep level position of the similar QDs buried by the substrates with distinct optical characteristics.

Acknowledgements

Author is grateful to Dr. Alexey G. Petrov for discussions stimulating the work and to Prof. Richard M. Martin for useful comments. The work was supported in part by RFBR grants No 99-02-18170 and No 96-15-96348.

References

[1] V. V. Rotkin and R. A. Suris, *Solid State Phys.* **36**, 1899–1905 (1994).

[2] A. B. Migdal, *Qualitative Methods in Quantum Theory* (Moskow: Nauka) 1975.

[3] S. V. Rotkin, unpublished.

8th Int. Symp. "Nanostructures: Physics and Technology"
St Petersburg, Russia, June 19–23, 2000

Spectroscopy of inhomogeneous strain in silicon-based quantum dots

A. Zaslavsky†, Jun Liu‡, B. R. Perkins† and L. B. Freund†
† Division of Engineering, Brown University, Providence, RI 02912, USA
‡ Dept. of Physics, Brown University, Providence, RI 02912, USA

Abstract. Resonant tunneling is employed to probe the inhomogeneous strain in silicon-based quantum dots. When submicron structures are etched from a *p*-Si/SiGe/Si double-barrier heterostructure, the resonant $I(V)$ peaks shift and develop a fine structure consistent with pronounced strain relaxation in the SiGe quantum well. We calculate the strain dependence on dot size by finite element techniques and convert the strain to an effective lateral confining potential. In sufficiently small dots, we find that the inhomogeneous strain confines carriers not only to the central core, as in GaAs-based dots, but also to a ring-like region at the perimeter. We probe the resulting density of states by magnetotunneling $I(V, B)$ measurements.

Introduction

When a semiconductor nanostructure, like a quantum wire or a quantum dot, is fabricated from strained epitaxially grown material, the originally homogeneous strain is replaced by geometry-specific strain gradients. The symmetry-based analytic treatment [1] for handling the biaxial strain in lattice-mismatched materials no longer suffices, particularly for quantum dots which lack translational symmetry altogether. Instead one turns to finite-element calculations of the strain field based on linear elastic models, but their applicability to structures whose size D might be down to tens of lattice constants is not self-evident. Thus, any experimental technique that is sensitive to inhomogeneous strains provides a valuable test bed for the validity of finite-element techniques for strained nanostructures – in our work, the experimental probe will be the resonant tunneling current-voltage $I(V)$ measurements.

Further, inhomogeneous strain in semiconductor nanostructures is taking on additional technological relevance, as advances in strained layer epitaxy and ongoing device miniaturization promise the arrival of deep submicron bandgap-engineered devices, such as strained Si/SiGe HBTs for high-frequency analog and digital applications. Particularly interesting is the use of strain-driven self-assembly of quantum dots in semiconductor lasers [2] to enhance gain and shift the lasing wavelength. In such devices, strain relaxation is the key to the size and morphology of the quantum dots, as well as the optical transition energies.

Finally, it is important to note that inhomogeneous strains in quantum nanostructures can contribute to carrier localization in unpredictable ways. Over the past decade, quantum dots have been extensively investigated as systems containing a few spatially confined charge carriers [3–5]. However, most of these experiments probed dots made from lattice-matched GaAs/AlGaAs heterostructures, in which the carriers are confined to the central region of the dot by a roughly parabolic lateral potential arising from the gate potential or the pinning of the Fermi level at the surface. In our strained Si/SiGe quantum dots, the inhomogeneous-strain-induced lateral confinement potential is nonmonotonic, leading to an effective potential minimum near the perimeter of the dot. For sufficiently small dots,

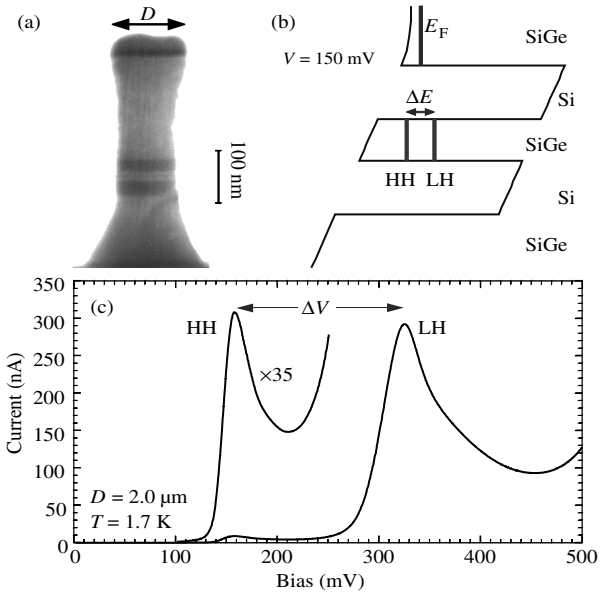

Fig. 1. (a) SEM micrograph of a representative double-barrier nanostructure with lateral dimension $D \sim 0.15\,\mu$m. (b) Self-consistent potential profile of the Si/SiGe double-barrier active region at $V = 150$ mV. (c) Resonant tunneling $I(V)$ of a large $D = 2\,\mu$m device at 1.7 K, with the HH peak magnified $\times 35$ for clarity.

this potential confines the ground state to a one-dimensional (1D) ring-like region near the perimeter − a new type of structure expected to have interesting magnetic properties.

1. Tunneling and strain in SiGe double-barrier microstructures

Our devices begin with p-Si/$Si_{1-x}Ge_x$/Si double-barrier heterostructures described in detail in previous publications [6, 7, 8]. They are grown on p-Si substrates, with an undoped active region consisting of Si barriers confining a $Si_{1-x}Ge_x$ QW that is 35 Å wide with Ge content $x = 0.25$ or 0.2 (corresponding to a lattice mismatch of ∼1 and ∼0.8% respectively). Outside the barriers are p-$Si_{1-x}Ge_x$ emitter and collector regions that serve as reservoirs for tunneling holes.

When a bias V is applied between the emitter and collector, the holes in the emitter tunnel via the quantized 2D hole subbands, subject to the usual energy E and transverse momentum $\mathbf{k}_\perp$ conservation rules [9]. In large devices, the strain in the SiGe well can be taken as biaxial and homogeneous, so the energies of the 2D subbands can be reliably calculated numerically [6]. Figure 1 shows an SEM photograph of a device, together with a self-consistent potential distribution in the active region under bias, and the $I(V)$ characteristic of a large $D = 2\,\mu$m Si/$Si_{0.75}Ge_{0.25}$ device at $T = 1.7$ K. The peaks correspond to tunneling through the two confined 2D subbands, labeled HH and LH for the heavy-hole and light-hole branches of the dispersion. The agreement with the predicted peak positions is excellent [6, 7], so the peak positions reflect the energies of the quantized states in the SiGe well. In particular, the energy separation ΔE between the HH and LH subbands arises in part from the strain-induced splitting, which lifts the HH-LH degeneracy in the SiGe valence band [1, 10]. Thus, any significant change in the strain should be reflected in ΔE.

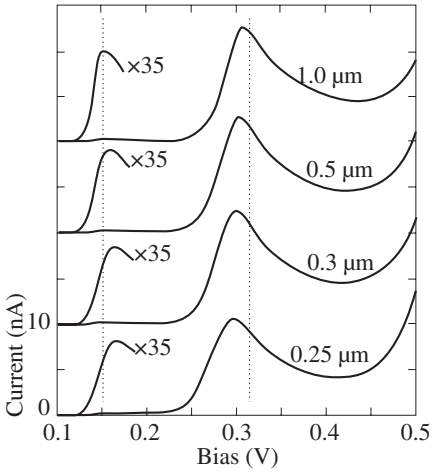

Fig. 2. $I(V)$ characteristics with nominal lateral diameters of $D = 1.0{-}0.25\,\mu$m at 1.7 K. Current scale corresponds to the smallest device, other curves are rescaled and the HH peaks magnified for clarity. Vertical lines mark the HH and LH peak positions in large devices.

2. Average strain relaxation in SiGe double-barrier microstructures

When a narrow mesa is etched through the active region of our devices, the biaxially compressed SiGe strained layers can relax by lateral displacement at the sidewall. We first observed this effect experimentally some years ago [7] and it has been confirmed by others [11]. Figure 2 shows the effect in a series of identically fabricated Si/$Si_{0.75}Ge_{0.25}$ devices with D ranging from 1 down to 0.25 μm. The $I(V)$ curves exhibit a consistent shift of HH and LH peaks towards each other as D decreases, even as the $I(V)$ lineshape remains largely unaffected. The effect is large, with changes in ΔE indicating a significant amount of strain relaxation.

We compared the strain relaxation inferred from the data in Fig. 2 to finite-element simulations based on a linear elastic model, in which the cylindrical structure was allowed to relax to a minimum energy configuration [12]. The average values of strain relaxation predicted by these calculations agree quite well with our experimental data, with the dominant radial strain component ϵ_{rr} relaxing to ~ 0.7 of the full lattice-mismatch strain when D falls to 0.3 μm. Interestingly, the simulated strain relaxation in the SiGe layers is non-monotonic in the radial direction $r_\perp$ and significant strain gradients exist throughout the SiGe well in sufficiently small structures, $D \leq 0.25\,\mu$m. The inhomogeneous strain leads to additional lateral quantization in the confined 2D subbands, which we first observed in [8].

3. Inhomogeneous strain in SiGe quantum dots

The calculated radial strain ϵ_{rr} in the SiGe QW and the corresponding strain-induced lateral potential for HH states are shown in Fig. 3 as a function of $r_\perp$ for $D = 0.1{-}0.2\,\mu$m devices with a $Si_{0.8}Ge_{0.2}$ well. The inset shows the calculation geometry and lateral displacement of the strained SiGe layers. First consider the radial strain $\epsilon_{rr}(r_\perp)$ curves at the top of Fig. 3. For $D = 0.2\,\mu$m, ϵ_{rr} decreases gradually with $r_\perp$ except for a region of increasing strain near the perimeter that extends ~ 100 Å and reaches $\epsilon_{rr} \sim 0.6$.

This strained ring-like region exists for all D [8], [12], but for devices much larger than

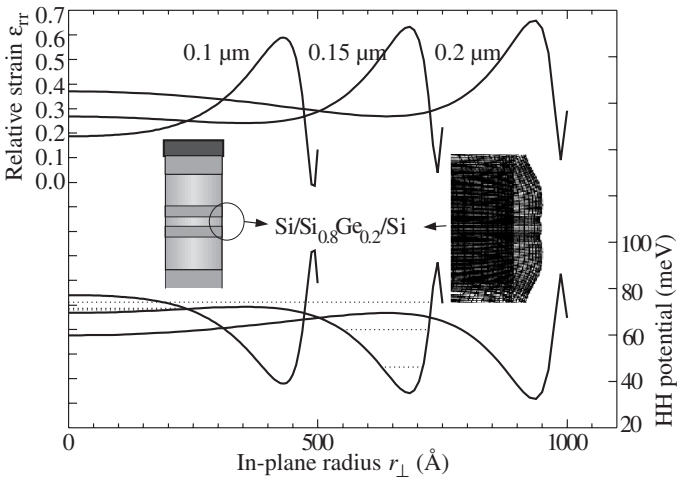

Fig. 3. The top curves show the calculated radial strain component $\epsilon_{rr}(r_\perp)$ for $D = 0.1{-}0.2\,\mu$m devices at the mid-plane of the $Si_{0.8}Ge_{0.2}$ well (full strain is $\epsilon_{rr} = 1$). Inset shows the magnified displacement of the finite-element mesh near the sidewall. The bottom curves are the corresponding in-plane confining potentials for the HH states as function of $r_\perp$. Dashed lines mark the confined ring subbands in a $D \sim 0.15\,\mu$m dot.

$D = 0.2\,\mu$m it can be taken as a perturbation to the inner core. On the other hand, in small devices, $D \leq 0.15\,\mu$m, the ring at the perimeter becomes the most highly strained region in the device. The corresponding confining potential for HH states is shown by the bottom set of curves in Fig. 3: in the smallest dots, the strain would confine holes to a 1D ring at the perimeter.

Figure 4 shows the HH $I(V)$ peak of a $D \sim 0.15\,\mu$m device fabricated from the $Si/Si_{0.8}Ge_{0.2}$ double-barrier material, together with a reference lineshape from a large device. The $I(V)$ lineshape exhibits very strong fine structure, corresponding to strong lateral quantization due to inhomogeneous strain [8]. A full-blown calculation of the expected density of states in such a quantum dot in the presence of the inhomogeneous strain is complicated by the anisotropy and nonparabolicity of the in-plane effective mass in the quantum well, but taking the in-plane HH effective mass $m^* \sim 0.25$ we obtain several radially quantized subbands in the perimeter ring separated by a few meV, see Fig. 3. Since quantized ring-like subbands overlap in energy with the states in the relaxed central core, they would be expected to contribute structure on top of the relatively smooth overall HH peak lineshape. The energy separation of the ring subbands extracted from the structure in the $I(V)$ agrees reasonably with the calculations of Fig. 3.

4. Magnetotunneling spectroscopy of strained SiGe quantum dots

The additional ring-like confinement of hole states in sufficiently small inhomogeneously strained SiGe quantum dots provides a new and interesting system for magnetic field effects. Figure 5(a) shows the evolution of the HH $I(V)$ peak fine structure in magnetic fields $B = 0{-}10$ T ($B \parallel I$), while Fig. 5(b) indicates the evolution of the $I(V)$ peaks converted to an energy scale. In the absence of inhomogeneous strain, the B field would compress the 2D subband density of states into Landau levels. Given a constant in-plane effective mass, as in n-GaAs/AlGaAs double-barrier structures, the Landau level separation would

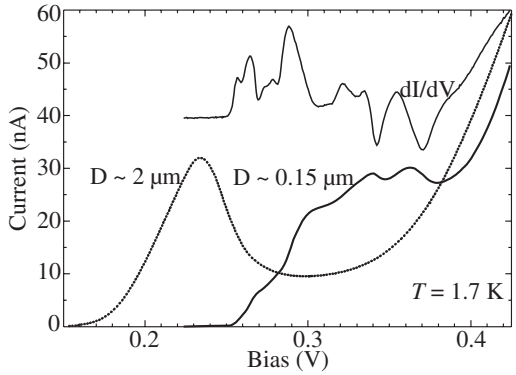

Fig. 4. HH resonant peak $I(V)$ and $\mathrm{d}I/\mathrm{d}V$ characteristics of a $D \sim 0.15\,\mu$m $Si/Si_{0.8}Ge_{0.2}$ dot. The dashed line shows the smooth HH $I(V)$ lineshape in a large device.

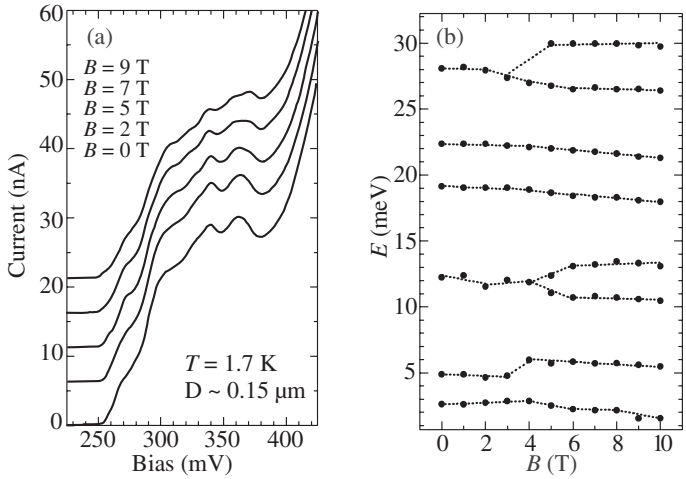

Fig. 5. (a) Evolution of HH $I(V, B)$ lineshape of the $D \sim 0.15\,\mu$m dot with B; (b) B-field-induced shifts and splittings in the density of states peaks in the dot.

be linear in B and the $I(V, B)$ lineshape would show equally spaced features falling on the usual Landau fan diagram [13]. Given the complex, nonparabolic dispersion of holes in SiGe quantum wells, the Landau level spectrum is quite complicated even in a uniformly strained well [14] and B-induced structure has only been seen experimentally at fairly large B [6]. The data in Fig. 5 shows rather complex behavior, with some of the peaks shifting towards lower energy with B, others appearing to repel each other, and some even splitting around $B \sim 5$ T. A theoretical analysis of ring-like hole states in a B field remains to be performed.

5. Conclusions

We have investigated the effects of size-induced strain relaxation in strained SiGe quantum dots. Our data indicate that large strain relaxation and nonomonotonic strain gradients appear in deep submicron structures, in agreement with finite element simulations. We also see evidence for confinement of carriers to ring-like regions at the perimeter due to inhomo-

geneous strain. Our measurements prove resonant tunneling to be a viable spectroscopic probe for strain effects in individual nanostructures.

Acknowledgements

The work at Brown has been supported by an NSF Career award for A. Z. (DMR-9702725), ONR (N00014-95-1-0239), the Sloan Foundation, and the MRSEC Program of the NSF (DMR-9632524).

References

[1] G. L. Bir and G. E. Pikus, *Symmetry and Strain-Induced Effects in Semiconductors*, New York, Wiley, 1974.

[2] D. Bimberg, M. Grundmann and N. N. Ledentsov, *Quantum Dot Heterostructures*, New York, Wiley, 1999.

[3] Bo Su, V. J. Goldman and J. E. Cunningham, *Science* **255**, 313 (1992).

[4] T. Schmidt, M. Tewordt, R. H. Blick *et al.*, *Phys. Rev. B* **51**, 5570 (1995).

[5] S. Tarucha, D. G. Austing, T. Honda *et al.*, *Phys. Rev. Lett.* **77**, 3613 (1996).

[6] A. Zaslavsky, D. A. Grützmacher, S. Lin *et al.*, *Phys. Rev. B* **47**, 16036 (1993).

[7] A. Zaslavsky, K. R. Milkove, Y. H. Lee *et al.*, *Appl. Phys. Lett.* **67**, 3921 (1995).

[8] C. D. Akyüz, A. Zaslavsky, L. Freund *et al.*, *Appl. Phys. Lett.***72**, 1739 (1998).

[9] S. Luryi, *Appl. Phys. Lett.* **47**, 490 (1985).

[10] For a concise treatment of SiGe, see R. People, *Phys. Phys. B* **32**, 1405 (1985).

[11] P. W. Lukey, J. Caro, T. Ziljstra, *et al.*, *Phys. Rev. B* **57**, 7132 (1998).

[12] H. T. Johnson, L. B. Freund *et al.*, *J. Appl. Phys.* **84**, 3714 (1998).

[13] See, for example, V. J. Goldman, D. C. Tsui and J. E. Cunningham, *Phys. Rev. B* **35**, 9387 (1987) and references therein.

[14] S.-R. Eric Yang, D. A. Broido and L. J. Sham, *Phys. Rev. B* **32**, 6630 (1985).